THE JOURNAL OF PHYSICAL CHEMISTRY C
A JOURNAL OF THE AMERICAN CHEMICAL SOCIETY

pubs.acs.org/JPCC

Article

Raman Spectroscopy and *In Situ* XRD Probing of the Thermal Decomposition of Sb_2Se_3 Thin Films

Arun Kumar, Vikash Kumar, Alessandro Romeo, Claudia Wiemer,* and Gino Mariotto*

Cite This: *J. Phys. Chem. C* 2021, 125, 19858−19865

Read Online

ACCESS | Metrics & More | Article Recommendations | Supporting Information

ABSTRACT: Sb_2Se_3 thin films have received increasing interest for their applications in optoelectronics. However, technological intervention demands a material-specific understanding of the reactivity to different environments. Both thermal annealing and laser irradiation carried out in an ambient atmosphere are expected to induce changes in the pristine crystallographic phase of Sb_2Se_3, causing the creation of additional secondary phases. Here, we investigate by means of Raman spectroscopy the effect of thermal annealing and laser irradiation at different fluencies on the structural and vibrational properties of Sb_2Se_3 thin films. The vacuum-annealed Sb_2Se_3 thin films at 290 °C and subjected to laser excitation power above 2 mW exhibit a secondary phase, revealing the occurrence of selenization. Further, *in situ* X-ray diffraction over a broad range of annealing temperatures in N_2 and ambient atmospheres was employed to study the structural properties of the Sb_2Se_3 thin films. *In situ* XRD performed in a N_2 atmosphere does not show the formation of the Sb_2O_3 cubic phase upon annealing until 500 °C. Conversely, a thermally activated systematic crystallization was observed upon annealing in an ambient atmosphere with the formation of the Sb_2O_3 phase in the temperature range between 280 and 420 °C, until the complete decomposition of the material at 500 °C. Further, the orientation of vertically stacked ($hk1$) planes remains unchanged under a N_2 atmosphere, while horizontally stacked ($hk0$) planes dominate the ($hk1$) planes under ambient atmospheres.

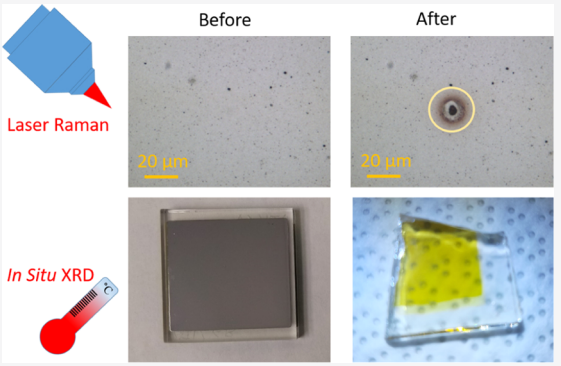

INTRODUCTION

Recently, there has been an increasing interest in semiconductor compounds A_2B_3 (A = As, Sb, Bi; B = S, Se, Te) due to their interesting chemical and physical properties, which make them candidates for applications such as thermoelectric devices,[1,2] topological insulators[3−6] superconductors,[3] energy storage devices,[7−9] and solar cells.[10−19] In particular, Sb_2Se_3 has gained much attention, especially with regard to photovoltaic applications.[14−20] This material has shown a conversion efficiency of about 9%,[21] which, however, is still lower than the theoretically predicted value of about 30%.[22−24] Thus, due to continuously improved conversion efficiency in solar cell research, it becomes very important to study this material in terms of chemical composition, thermal stability, oxidation, phase transformation, and atomic interdiffusion. This gives an opportunity to study this material extensively.

Importantly, the investigation of the above-mentioned compounds is not straightforward due to their chemical instability. Raman spectroscopy has attracted significant attention in investigating semiconductor compounds.[25−29] These materials can be transformed when their temperature is increased by absorbing incident laser radiation. The temperature rise is affected by quantities such as power, stimulated surface area, exposure time, the wavelength of laser radiation, reflectivity, and thermal conductivity of the sample.

The binary Sb−Se system is stable in the Sb_2Se_3 chemical composition only if arranged in the orthorhombic structure (space group *Pnmb*, with a = 11.62 Å, b = 11.77 Å, and c = 3.962 Å).[29] This is of key importance because it implies that neither structural polymorphs nor appreciable amounts of secondary phases with different chemical compositions are expected in this system, thus simplifying its technological applications.

Group theory analysis of the orthorhombic Sb_2Se_3 with four formula units per unit cell of the *Pnmb* space group results in 60 different phonon modes. These modes are distinguished as three acoustic modes, 57 optical modes, of which 30 are Raman active modes, 22 are IR active modes, and five are silent modes.[30−33] The occurrence of all 30 anticipated Raman modes in the frequency region below 750 cm^{-1} requires proper investigation *via* high-resolution low-frequency micro-Raman spectroscopy. Till now, to the best of our knowledge, only a few similar studies have been carried out on Sb_2Se_3

Received: June 8, 2021
Published: September 8, 2021

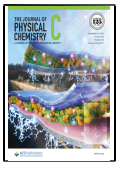

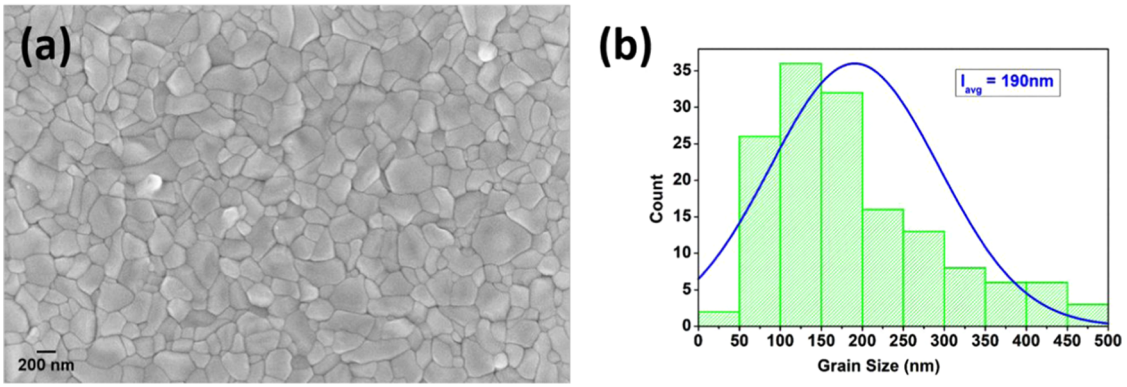

Figure 1. (a) Plan-view SEM image of a thin film and (b) the corresponding histogram of the grain size distribution for the as-deposited Sb_2Se_3 thin films.

materials,[29,31] and so it becomes necessary to understand the possible limitations (such as thermal annealing, stacking plane orientation, *etc.*) in achieving the wide range of applications of this ideal material. Raman spectroscopy allows for the unambiguous identification of its dominant phases. Conversely, this does not happen for X-ray diffraction (XRD) due to the reflection overlapping problem.

In this paper, we report on the results of the low-frequency micro-Raman spectroscopy and *in situ* XRD investigations during thermal annealing of Sb_2Se_3 thin films. Raman spectra of thermally annealed Sb_2Se_3 were first analyzed, followed by the systematic experimental study of the micro-Raman spectroscopy with special attention to the laser power impinging on the sample surface. The discrepancy related to the band positions and their identification with the reported literature prompted a more detailed investigation of the Raman response of Sb_2Se_3 from our side, under both thermal treatment and laser irradiation conditions. Considering the available literature, we offer a thorough discussion on the vibrational properties of Sb_2Se_3. The correlation between the experimental data obtained by both characterization techniques allows for a better understanding of physico-chemical properties of the Sb_2Se_3 thin films and the optimal thermal conditions. The results would provide a foundation on Raman and XRD studies of Sb_2Se_3 thin films.

EXPERIMENTAL SECTION

Thin-Film Deposition. Antimony selenide (Sb_2Se_3) thin films, suitable for solar cells, were synthesized in a superstrate configuration by a low-temperature vacuum evaporation (VE) process. To study the Sb_2Se_3, we started from a metal-coated glass/indium tin oxide (ITO)/ZnO/CdS/Sb_2Se_3 stack. A 400 nm thick indium tin oxide (ITO) film was deposited on a 3 × 3 cm^2, 4 mm thick, soda-lime glass by radio frequency (RF)-magnetron (5 Pa) sputtering with 90% In_2O_3 and 10% SnO_2 target in an Ar + 2% O_2 atmosphere and with the substrate temperature of 400 °C. The ITO layer was covered by a 100 nm thick i-ZnO film, deposited by RF magnetron sputtering in an atmosphere of Ar + 2% O_2 with a substrate temperature of 400 °C. The stack was then annealed under vacuum at 10^{-4} Pa at 450 °C. CdS was deposited on the ITO/ZnO stack by thermal evaporation at a pressure of 10^{-4} Pa, substrate temperature of 150 °C, and thickness of 150 nm. After deposition, the layer was annealed under vacuum at 450 °C to improve its crystalline structure. The samples were then transferred into another vacuum evaporation unit (Homemade System), where Sb_2Se_3 was deposited on the glass/ITO/ZnO/CdS stack. A 1 μm thick absorber was deposited at a base pressure of 3.6 × 10^{-4} Pa and with a substrate temperature of 290 °C. Sb_2Se_3 lumps were heated in a graphite crucible at the temperature range of 700−800 °C to be evaporated at a deposition rate of approximately 0.28 nm/s. The final stacking becomes glass/ITO/ZnO/CdS/Sb_2Se_3 with a thickness of 400 nm/100 nm/150 nm/1 μm, respectively. Post deposition treatment was applied by annealing the samples in air at 190, 290, and 390 °C for about 30 min.

Characterization. Low-frequency micro-Raman experiments were conducted on both as-deposited and annealed Sb_2Se_3 samples by means of an He−Ne laser (λ_{exc} = 633 nm) coupled to a single-stage Raman spectrometer (Thermo Scientific DXR2) and a charge-coupled device, thermoelectrically cooled. All measurements were carried out at room temperature (RT). The average spectral resolution was 4 cm^{-1}, and the lowest resolvable frequency was 30 cm^{-1}. The laser was focused on the sample surface using a 50× objective (long working distance) having a numerical aperture close to 0.5. The size of the laser spot on the sample surface was approximately 2 μm, and the position of the sample was adjusted using the motorized stage. The penetration depth of the red laser beam (*i.e.*, λ = 633 nm) into our stacked structure is expected to be less than 1 μm. Taking into consideration the thermal and photosensitivity of the Sb_2Se_3 material, the incident laser power was initially set equal to 0.1 mW, corresponding to an energy density of about 10^3 W/cm^2 deposited on the sample surface, and then moved up stepwise to higher power levels. This approach allowed us to locally obtain the phase transformation of the sample.

In situ grazing incidence X-ray diffraction (XRD) experiments during the thermal treatment were performed with a laboratory instrument (HRXRD IS2000) equipped with a sealed Cu Kα tube, a four-circle goniometer, a single point (NaI) detector, and a position-sensitive Inel gas detector able to collect data under an angle of 120°. The angle of incidence was set at ω = 2°. A separate isothermal heat treatment with a Domed Hot Stage (DHS) 1100 (Anton Paar GmbH, Graz, Austria) with a polymer dome was employed under a N_2 flux flow and ambient atmosphere. Precise alignment on the sample surface was performed with the scintillator detector, and the acquisition of the diffracted intensity was performed with the position-sensitive detector. The experimental XRD curves were analyzed by a best-fit procedure based on the Rietveld method.[34]

https://doi.org/10.1021/acs.jpcc.1c05047
J. Phys. Chem. C 2021, 125, 19858−19865

The surface image of Sb_2Se_3 thin film was taken by a field emission scanning electron microscope (SEM, Zeiss, SUPRA 40).

The elemental composition of the Sb_2Se_3 thin films was measured using a total reflection X-ray fluorescence (TXRF) spectrometer equipped with a Mo Kα radiation source.

The crystal structure was produced by VESTA software.[35]

RESULTS AND DISCUSSION

The typical morphology revealed by the SEM micrograph of the as-grown Sb_2Se_3 thin film is shown in Figure 1a. The Sb_2Se_3 layer was observed to be uniformly dense and with completely intact grains without cracks and voids. The grain size of the as-deposited Sb_2Se_3 layer was found to be in the range of about 30−500 nm interconnected with each other, with an average grain size, I_{avg}, of about 190 nm (see Figure 1b). Such a surface, with large grains and compact morphology, is suitable for the construction of thin-film solar cells.

Figure 2 presents the experimental Raman spectra of Sb_2Se_3 thin films subjected to different annealing temperatures carried out under red light excitation (λ_{exc} = 633 nm). Their spectral intensity shows a pronounced dependence on the annealing temperature. In our case, the Raman spectra display peaks at about 43, 54, 82, 103, 118, 129, 153, 191, and 210 cm^{-1} for all of the prepared samples. The peaks at around 153, 191, and 210 cm^{-1} are commonly reported and assigned to the Sb_2Se_3 phase.[29,36] Moreover, two strong low-frequency Raman peaks are observed for the first time at 43 and 54 cm^{-1}. These peaks have not been reported in the literature previously. They show full widths at half-maximum (FWHMs) of around 4 cm^{-1}. Such narrow FWHMs suggest a long lifetime of the optical phonon vibrational modes.[37] These two modes could be considered as strong Sb−Se modes. Low-frequency Raman peaks do not show any significant change in the spectral shape at the higher annealing temperature. This indicates that no structural transformation occurred at this level, suggesting a highly stable crystalline structure. We perform this analysis based on a similar material Sb_2S_3.[28,38,39] In this context, the displacement of the vibrational modes with low frequencies (<150 cm^{-1}) should be mainly attributed to the movement of heavy Sb atoms.[39] The Raman modes at 82 and 118 cm^{-1}, which are related to the Se−Se bending,[36] show a well-defined blue shift of about 2 cm^{-1} following the increase of the annealing temperature (190−390 °C) of the Sb_2Se_3 thin films. The small shoulders observed at about 103 and 129 cm^{-1} are assigned to the Se_6 ring of rhombohedral Se.[40] All these spectral features remain the same even at the highest annealing temperature. The Raman peak at about 153 cm^{-1} has been attributed to the A_{2u} mode of the Sb−Sb bond,[41] while the peaks at about 191 and 210 cm^{-1} are commonly assigned to the A_g mode of the Sb−Se−Sb bending vibrations of Sb_2Se_3.[42] The Raman spectra of the as-deposited Sb_2Se_3 thin-film overlap well with the sample annealed at 190 °C in air, which means that the microstructure of the Sb_2Se_3 thin films has not been altered by annealing temperature up to 190 °C.

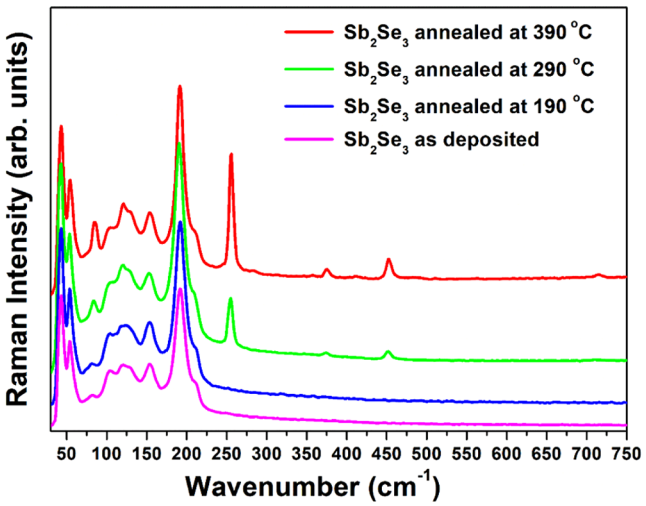

Figure 2. Raman spectra of the as-deposited Sb_2Se_3 layer as well as of Sb_2Se_3 layers annealed at some increasing temperatures.

Further, it should be noted that no peak in the spectral region above 220 cm^{-1} was observed until 190 °C annealing temperature. The appearance of relatively less intense peaks at about 255, 375, 452, and 715 cm^{-1} in the spectra of the samples vacuum-annealed at 290 °C is a clear evidence of the formation of α-Sb_2O_3. The peak at about 255 cm^{-1} was commonly reported in the Raman studies of Sb_2Se_3,[17,43−45] and it was later studied and suggested to be related to Sb_2O_3.[28,29] While other researchers have assigned this band to the stretching vibrations of the Se−Se bond in Se chains and Se_8 rings[17] and the ^1B_g mode of antisymmetric stretching vibrations of the Sb_2Se_3 phase.[42] The assigned Se−Se bonds at the lower deposition temperature and the achieved structural ordering with the increment in the temperature,[17] were not observed in our case. As the annealing temperature increases, along with the appearance of the 255 cm^{-1} peak, other peaks (375, 452, and 715 cm^{-1}) were also detected, whose intensities followed the increase in the intensity of the 255 cm^{-1} one, confirming that they are possibly related. In fact, the positions of these bands match the assigned ones to α-Sb_2O_3.[29] Additionally, two very less intense bands at 283 and 411 cm^{-1} were also observed in the spectrum of the sample annealed at 390 °C, which could be due to the β-Sb_2O_3 secondary phase.[46] However, at lower annealing temperatures, we did not observe these bands. Thus, we conclude that the increase in the annealing temperature is responsible for the structural ordering and oxidation of the films. We observed and confirmed the secondary phases with a temperature increase at the local area scale using the 633 nm laser line instead of the 442 nm.[29,31,46] On the other hand, we found that the Sb−Se bonds were dominant in the Sb_2Se_3 thin films, and they were quite stable at the various annealing temperatures.

Laser Irradiation Effects. After having analyzed the overall room temperature Raman spectrum from samples subjected to different annealing temperatures, we next examined the Raman spectra of Sb_2Se_3 thin films as a function of the excitation power. The low thermal conductivity of Sb_2Se_3[47,47] helps in the understanding of its Raman spectra recorded under different excitation powers due to the laser heating effect. To have a detailed understanding of the structural changes, occurring in Sb_2Se_3 films irradiated with increasing laser power, the relative intensities, the positions and the spectral changes of its vibrational modes were investigated. After characterization of the as-deposited film, the same 633 nm laser line was used (at a higher power level) to locally heat and structurally modify the Sb_2Se_3 thin-film surface. In general, focused laser irradiation can induce local heating up to several hundreds of degrees, depending on the

https://doi.org/10.1021/acs.jpcc.1c05047
J. Phys. Chem. C 2021, 125, 19858−19865

energy density deposited on the sample surface. Since the Sb−Se material has a narrow thermodynamic growth window, the phase transition can be achieved by local laser heating of the surface. To confirm the possibility of phase transformation by laser annealing, Raman spectra were collected after carefully varying the laser power intensity in the range of 0.1−8 mW in steps, corresponding to an energy density deposited on the sample surface, ranging from 10^3 to 10^5 W/cm^2, and keeping the same time of integration (see Figure S1, Supporting Information).

Figure 3 shows the Raman spectra of Sb_2Se_3 peaks at about 43, 54, 82, 103, 118, 129, 153, 191, and 210 cm^{-1} at all laser

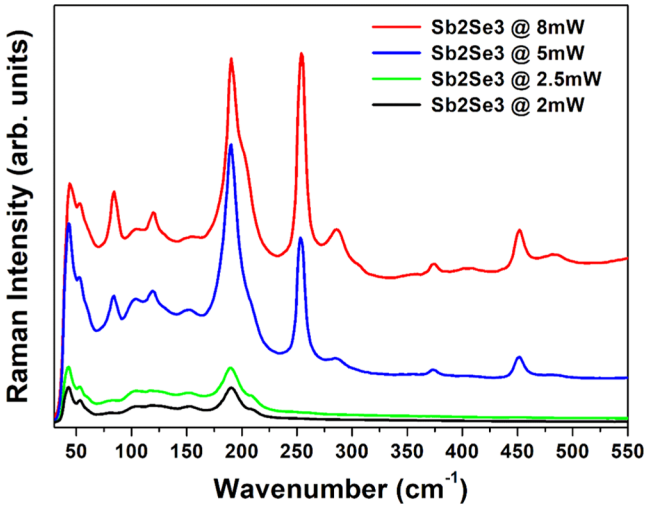

Figure 3. Raman Spectra of the as-deposited Sb_2Se_3 layer, as well as Sb_2Se_3 layers, subjected to different laser excitation powers.

power densities. The spectra are in good agreement with the one earlier recorded from the as-deposited Sb_2Se_3 thin film under the lowest power excitation and with those reported in the literature.[29,31] Next, the spectra exhibit a clear peak located at 190 cm^{-1} that remains, within the experimental error, stable in position and integrated intensity. However, its full width at half-maximum (FWHM) decreases as we increase the laser power density. The well-known laser heating effect always causes anharmonic effects in solids, evidenced by a broadening and a peak red shift of the Raman bands,[27] and simultaneously, under high-power or prolonged laser irradiation, structural transitions and crystalline changes may occur due to long-range ordering, as well as local or macroscopic ordering.[28] At first glance, one might think that the decrease of the FWHM of the peak at 190 cm^{-1} is related to the local annealing of the Sb_2Se_3 phase, which results in an improvement in the crystalline quality of the material. However, if this would be the case, one would expect a gradual increase in intensity throughout the experiment, which was not observed in our case, suggesting that the crystalline quality of the materials reduces. Further, a small band located at about 252 cm^{-1} was observed, which became well-defined and prominent with increasing laser power. The intensity of the band increases significantly and becomes highest with 8 mW laser power. Along with 252 cm^{-1}, other well-defined bands at 374, 451, and 712 cm^{-1} show the same behavior (see Figure S1, Supporting Information). The bands could be related to the secondary phase of Sb_2Se_3, which is α-Sb_2O_3. Raman bands at about 286 and 482 cm^{-1} were observed at higher laser power densities and have not been reported in the literature for this type of material so far. These bands could also be originated from the α-Sb_2O_4 secondary phase.[46] At the full power of 8 mW, the Sb_2O_3 phase seems to become the most dominant one in the local area. Nevertheless, no Raman peak related to α-Sb_2O_3 was observed in this experiment until the excitation power of 2 mW. This may result from the out of resonance enhancement due to the large energy difference between the photon energy of the excitation laser and the Sb−Se band gap energy. To recheck the investigated sample for its phase transition, optical microscopy imaging was performed. The optical images of the laser-irradiated region with a yellow circle are shown in Figure S2. The optical images demonstrate that the surface is not damaged up to 2 mW. Beyond 2.5 mW, the film became more and more damaged, and it can be evidently observed from the optical image. At higher power irradiation, irreversible damage of the Sb_2Se_3 thin layer was observed. This phenomenology explicitly gives us the idea to clearly differentiate the transformed phases and, in the meantime, it provides a clear indication that probing with low power is mandatory to keep the phase stable.

***In Situ* XRD.** Further, to confirm our findings, *in situ* XRD measurements were performed on samples thermally annealed from room temperature (RT) to 500 °C in order to thoroughly investigate the phase transformation of the Sb_2Se_3 thin films. The sample was heated at the respective temperatures for 6 min, and then an XRD pattern was recorded for 3 min. The ramp between each temperature was 50 °C/min. The XRD patterns were recorded at RT and then from 40 to 500 °C with steps of 20 °C. After the annealing, the pattern of the sample that reached 500 °C was also registered at room temperature. Figure 4 shows the XRD analysis performed in a N_2 atmosphere. Figure 4a depicts the orthorhombic *Pnma* crystallographic structure of Sb_2Se_3. The XRD pattern of the as-deposited sample is shown in Figure 4b. This pattern has been registered with and without the dome, to appreciate the contribution of the spurious peaks due to the diffraction from the dome. All of the remaining identified peaks belong to the orthorhombic structure of Sb_2Se_3.[48] The XRD patterns recorded during the *in situ* annealing are presented in the intensity map in Figure 4c. No additional peak was found to develop during the annealing, and the only modification of the XRD patterns consists of slight variations of peak intensities and the shift of the peak position due to the thermal expansion at different temperatures. No additional patterns related to the secondary or the Sb_2O_3 phase were detected. Further, no significant difference in the intensity of the (hk1) (mainly (211) and (221)) and (hk0) (mainly (230) (330)) planes was observed, and it is an indicative parameter for the quality of the film; (hk1) planes (vertically stacked) were always dominant over (hk0) planes (horizontally stacked). It was found that the efficiency of photovoltaic solar cells is proportional to the intensity of the (hk1) planes, as the carrier moves along these vertically stacked planes exhibiting better charge collection.[23] Figure 4d shows the pattern obtained after annealing up to 500 °C. The comparison with the pattern of the as-deposited material confirms that the Sb_2Se_3 structure did not evolve, with the only variation related to the increasing of some peak intensities, without the development of preferential orientation. The experimental results from thermal annealing of Sb_2Se_3 thin films under a N_2 atmosphere suggest a structural ordering in terms of morphology (see Figure S3, Supporting Information). The grain sizes were found in the range of about

https://doi.org/10.1021/acs.jpcc.1c05047
J. Phys. Chem. C 2021, 125, 19858−19865

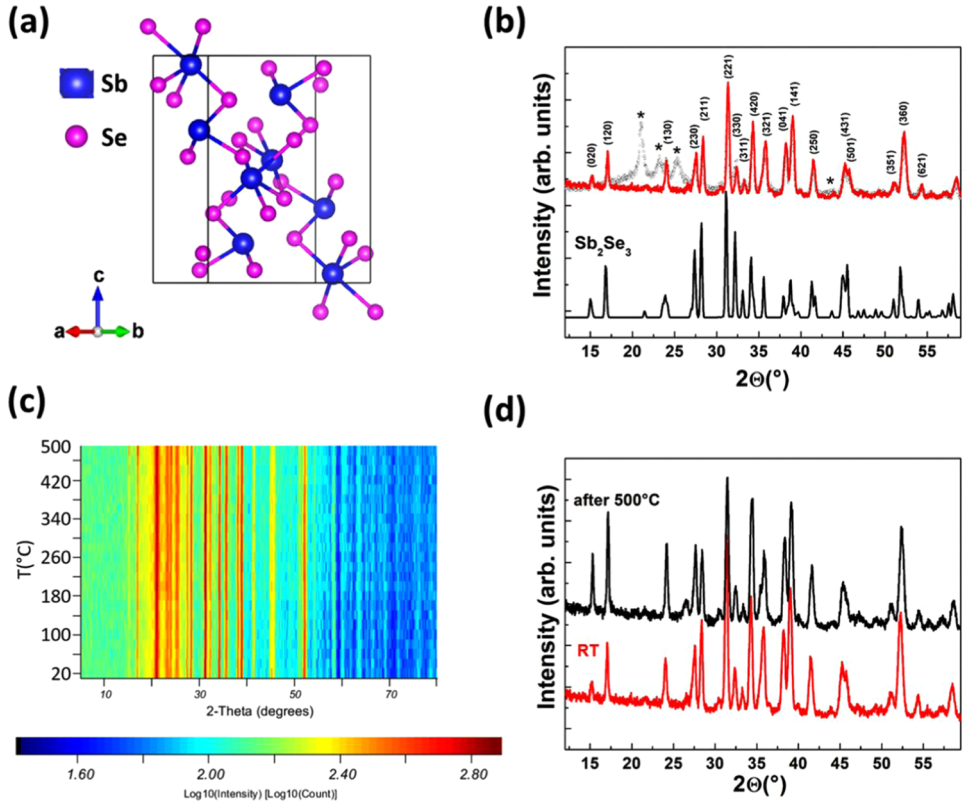

Figure 4. XRD study performed in a N_2 atmosphere. (a) Unit cell structure diagram of Sb_2Se_3. (b) XRD pattern of the as-deposited sample, registered without (red line) and with (black dots) dome. The asterisk (*) indicates the peaks due to scattering from the dome. The pattern is compared with the Sb_2Se_3 powder structure, as reported in the database.[48] (c) Intensity map of the XRD patterns as a function of temperature as registered during the *in situ* annealing. (d) Comparison of the XRD patterns before and after the annealing procedure.

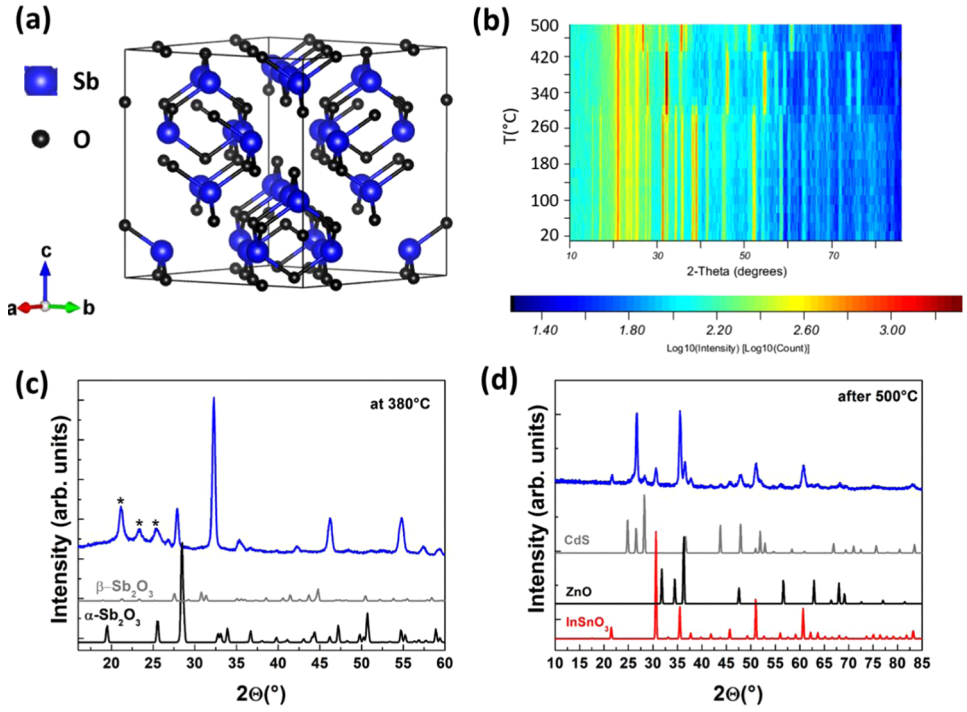

Figure 5. XRD study performed in air. (a) Unit cell structure diagram of Sb_2O_3. (b) Intensity maps of XRD patterns as a function of annealing temperature. (c) XRD patterns registered at 380 °C. The * mark indicates the peaks belonging to scattering from the dome. The pattern is compared to those of α and β Sb_2O_3, as reported in the database.[49,50] (d) XRD pattern after annealing up to 500 °C: the patterns are compared with those of $InSnO_3$, ZnO, and CdS.[51−53]

https://doi.org/10.1021/acs.jpcc.1c05047
J. Phys. Chem. C 2021, 125, 19858−19865

100−600 nm interconnected with each other without forming any isolated agglomerates of grains, with an average grain size of about 270 nm. The morphological ordering in terms of increase in grain size, without any additional isolated agglomerates of grains, is an important factor to enhance the performances of the resulting solar cells.[28]

Additionally, the TXRF spectrum related to as-deposited and post-*in-situ*-annealed Sb_2Se_3 films mainly shows the elemental presence of Sb and Se (see Figure S4, Supporting Information). No additional element was detected.

The same *in situ* XRD study was performed in air. The XRD analysis is presented in Figures 5 and S5. Figure 5a represents the diagram of the cubic structure of Sb_2O_3. The intensity map during the *in situ* XRD study is presented in Figure 5b. The disappearance of some peaks and the development of new ones are noticeably visible. The details of all of the registered diffraction patterns are presented in the Supporting Information (see Figure S5). From the registered patterns, three regions can be easily distinguished: (i) from room temperature to 300 °C, (ii) from 300 to 420 °C, (iii) and from 420 to 500 °C. In the first region, the Sb_2Se_3 structure was found to be maintained, with only a slight modification of peak intensities. In the second region, we observed a gradual disappearance of the Sb_2Se_3 structure and the development of Sb_2O_3, starting from 280 °C (see Figure S5, Supporting Information). In this temperature regime, Se evaporated and the remaining Sb was fully oxidized. Figure 5c shows the *in situ* pattern acquired at 380 °C; this pattern can be definitely ascribed to α-Sb_2O_3, with a minor component that can be due to β-Sb_2O_3.[49,50] The obtained results are in corelation with the Raman findings, where we observed the initial development of the Sb_2O_3 phase from the sample annealed at 290 °C. This result is further evidence that with the increase of the annealing temperature, Sb_2Se_3 decomposes to form Sb_2O_3. After 420 °C, the XRD pattern drastically changes, and the Sb_2O_3 completely evaporates. Figure 5d exhibits the pattern after 500 °C and is fully compatible with the $InSnO_3$/ZnO/CdS substrates peaks.[51−53] The optical image of before and after annealing of the substrate is shown in the Supporting Information (see Figure S6).

Finally, we observed a significant variation in the intensity of the (*hk*1) (mainly (211) and (221)) and (*hk*0) (mainly (230) (330)) planes as a function of the temperature under an ambient atmosphere. The intensity of the (*hk*0) planes starts increasing at RT; it completely dominates over the range of temperature, and (211) and (221) planes completely terminate at 320 and 340 °C (see Figure S5, Supporting Information), indicative of a temperature-induced structural transition. This suggests that the annealing in air facilitates the nucleation and growth of (*hk*0) plane-oriented grains while suppressing the (*hk*1) plane-oriented grains growth. The (*hk*1)-oriented grains were dominantly terminated with (*hk*0) planes, which had lower surface energies, and thus these (*hk*1) planes completely vanish upon annealing at higher temperatures.

CONCLUSIONS

In summary, we have thoroughly analyzed both the Raman spectrum of Sb_2Se_3, which varies significantly with the annealing temperature as well as the excitation power, and the *in situ* XRD pattern recorded under either a N_2 or an ambient atmosphere. The observed changes are discussed in terms of the intensity, FWHM, and shift of the main spectral components. The occurrence of secondary phases of material has been inferred in terms of the new Raman peaks observed, which allowed for their definite identification. Moreover, based on our results, we propose to use an annealing temperature below 280 °C and the excitation laser power in the range of 0.1−2 mW to take advantage of the Sb_2Se_3 layer without losing the Se in thin-film solar cell materials preparation. *In situ* XRD results have revealed that a structural rearrangement and formation of additional secondary phases or Sb_2O_3 could be avoided under N_2 atmospheres, as no significant change in the vertically stacked (*hk*1) planes was noticed. Further, a drastic change in the structural patterns starts appearing at about 280 °C, leading to the formation of additional phases of Sb_2O_3 and loss of Se under an ambient atmosphere. Moreover, the horizontally stacked (*hk*0) planes were found to be dominated over the vertically stacked (*hk*1) planes during the thermal treatment in an ambient atmosphere. An important remark from our work is related to the stability of the Sb_2Se_3 compound, which is directly dependent on high-energy conditions, like excitation laser power or temperature. These conditions can easily lead to the formation of the Sb_2O_3 compound. Thus, these factors should be taken into account during the synthesis processes. Further, this would help the researchers to improve the device efficiency of the Sb_2Se_3 solar cells.

ASSOCIATED CONTENT

Supporting Information

The Supporting Information is available free of charge at https://pubs.acs.org/doi/10.1021/acs.jpcc.1c05047.

Raman spectra of the as-deposited Sb_2Se_3 thin-film excited under different laser powers between 0.1 and 8 mW; optical images of the as-deposited Sb_2Se_3 thin film and after irradiation at different laser excitations: 2.5, 5, and 8 mW; plan-view SEM image of the thin film and the corresponding histogram of the grain size distribution for the *in-situ*-annealed Sb_2Se_3 thin films under a N_2 atmosphere; TXRF spectrum on as-deposited and post-*in-situ*-annealed Sb_2Se_3 thin films; *in situ* XRD in air of the as-deposited Sb_2Se_3 thin film at different annealing temperatures; and optical image of the as-deposited Sb_2Se_3 sample, after annealing at 500 °C in a N_2 atmosphere and after annealing at 500 °C in the ambient atmosphere (PDF)

AUTHOR INFORMATION

Corresponding Authors

Claudia Wiemer − *CNR Institute for Microelectronics and Microsystems, 20864 Agrate Brianza, MB, Italy*; Email: claudia.wiemer@mdm.imm.cnr.it

Gino Mariotto − *Micro Raman Spectroscopy Laboratory, Department of Computer Science, University of Verona, 37134 Verona, Italy*; orcid.org/0000-0002-0035-1404; Email: gino.mariotto@univr.it

Authors

Arun Kumar − *Micro Raman Spectroscopy Laboratory, Department of Computer Science, University of Verona, 37134 Verona, Italy; CNR Institute for Microelectronics and Microsystems, 20864 Agrate Brianza, MB, Italy*; orcid.org/0000-0002-6333-2198

Vikash Kumar − *Laboratory for Photovoltaics and Solid State Physics, Department of Computer Science, University of Verona, 37134 Verona, Italy*

Alessandro Romeo − *Laboratory for Photovoltaics and Solid State Physics, Department of Computer Science, University of Verona, 37134 Verona, Italy*

Complete contact information is available at: https://pubs.acs.org/10.1021/acs.jpcc.1c05047

Notes

The authors declare no competing financial interest.

■ ACKNOWLEDGMENTS

The authors would like to acknowledge Conferenza dei Rettori delle Università Italiane (CRUI) for supporting the open access.

■ REFERENCES

(1) Ovsyannikov, S. V.; Shchennikov, V. V. High-pressure routes in the thermoelectricity or how one can improve a performance of thermoelectrics. *Chem. Mater.* **2010**, *22*, 635−647.

(2) Kim, H. C.; Oh, T. S.; Hyun, D. B. Thermoelectric properties of the p-type Bi2Te3-Sb2Te3-Sb2Se3 alloys fabricated by mechanical alloying and hot pressing. *J. Phys. Chem. Solids* **2000**, *61*, 743−749.

(3) Qi, X. L.; Zhang, S. C. Topological insulators and superconductors. *Rev. Mod. Phys.* **2011**, *83*, 1057.

(4) Chen, Y. L.; Analytis, J. G.; Chu, J. H.; Liu, Z. K.; Mo, S. K.; Qi, X. L.; Zhang, H. J.; Lu, P. H.; Dai, X.; Fang, Z.; et al. Experimental realization of a three-dimensional topological insulator, Bi2Te3. *Science* **2009**, *325*, 178−181.

(5) Zhang, H.; Liu, C.-X.; Qi, X.-L.; Dai, X.; Fang, Z.; Zhang, S.-C. Topological insulators in Bi2Se3, Bi2Te3 and Sb2Te3 with a single Dirac cone on the surface. *Nat. Phys.* **2009**, *5*, 438−442.

(6) Kumar, A.; Cecchini, R.; Locatelli, L.; Wiemer, C.; Martella, C.; Nasi, L.; Lazzarini, L.; Mantovan, R.; Longo, M. Large-Area MOVPE Growth of Topological Insulator Bi2Te3 Epitaxial Layers on i-Si(111). *Cryst. Growth Des.* **2021**, *21*, 4023−4029.

(7) Malligavathy, M.; Ananth Kumar, R. T.; Das, C.; Asokan, S.; Pathinettam Padiyan, D. Growth and characteristics of amorphous Sb2Se3 thin films of various thicknesses for memory switching applications. *J. Non-Cryst. Solids* **2015**, *429*, 93−97.

(8) Ni, J.; Bi, X.; Jiang, Y.; Li, L.; Lu, J. Bismuth chalcogenide compounds Bi2 × 3 (X = O, S, Se): Applications in electrochemical energy storage. *Nano Energy* **2017**, *34*, 356−366.

(9) Ge, P.; Cao, X.; Hou, H.; Li, S.; Ji, X. Rodlike Sb2Se3 Wrapped with Carbon: The Exploring of Electrochemical Properties in Sodium-Ion Batteries. *ACS Appl. Mater. Interfaces* **2017**, *9*, 34979−34989.

(10) Tang, R.; Wang, Z.; Li, W.; Feng, L.; Zhang, J.; Wu, L.; Li, B.; Zeng, G.; Wang, W. Bi2Te3 thin films prepared by co-evaporation for CdTe thin film solar cells. *Sol. Energy Mater. Sol. Cells* **2014**, *121*, 92−98.

(11) Escorcia-García, J.; Becerra, D.; Nair, M. T. S.; Nair, P. K. Heterojunction CdS/Sb2S3 solar cells using antimony sulfide thin films prepared by thermal evaporation. *Thin Solid Films* **2014**, *569*, 28−34.

(12) Fukumoto, T.; Moehl, T.; Niwa, Y.; Nazeeruddin, M. K.; Gratzel, M.; Etgar, L. Effect of interfacial engineering in solid-state nanostructured Sb2S3 heterojunction solar cells. *Adv. Energy Mater.* **2013**, *3*, 29−33.

(13) Messina, S.; Nair, M. T. S.; Nair, P. K. Solar cells with Sb2S3 absorber films. *Thin Solid Films* **2009**, *517*, 2503−2507.

(14) Ngo, T. T.; Chavhan, S.; Kosta, I.; Miguel, O.; Grande, H. J.; Tena-Zaera, R. Electrodeposition of antimony selenide thin films and application in semiconductor sensitized solar cells. *ACS Appl. Mater. Interfaces* **2014**, *6*, 2836−2841.

(15) Yuan, C.; Jin, X.; Jiang, G.; Liu, W.; Zhu, C. Sb2Se3 solar cells prepared with selenized dc-sputtered metallic precursors. *J. Mater. Sci. Mater. Electron.* **2016**, *27*, 8906−8910.

(16) Choi, Y. C.; Mandal, T. N.; Yang, W. S.; Lee, Y. H.; Im, S. H.; Noh, J. H.; Seok, S. Il Sb2Se3 -Sensitized Inorganic-Organic Heterojunction Solar Cells Fabricated Using a Single-Source Precursor. *Angew. Chem.* **2014**, *126*, 1353−1357.

(17) Li, Z.; Chen, X.; Zhu, H.; Chen, J.; Guo, Y.; Zhang, C.; Zhang, W.; Niu, X.; Mai, Y. Sb2Se3 thin film solar cells in substrate configuration and the back contact selenization. *Sol. Energy Mater. Sol. Cells* **2017**, *161*, 190−196.

(18) Kumar, V.; Artegiani, E.; Kumar, A.; Mariotto, G.; Piccinelli, F.; Romeo, A. Effects of post-deposition annealing and copper inclusion in superstrate Sb2Se3 based solar cells by thermal evaporation. *Sol. Energy* **2019**, *193*, 452−457.

(19) Chen, C.; Zhao, Y.; Lu, S.; Li, K.; Li, Y.; Yang, B.; Chen, W.; Wang, L.; Li, D.; Deng, H.; et al. Accelerated Optimization of TiO2/Sb2Se3 Thin Film Solar Cells by High-Throughput Combinatorial Approach. *Adv. Energy Mater.* **2017**, *7*, No. 1700866.

(20) Hu, X.; Tao, J.; Chen, S.; Xue, J.; Weng, G.; Kaijiang; Hu, Z.; Jiang, J.; Chen, S.; Zhu, Z.; et al. Improving the efficiency of Sb2Se3 thin-film solar cells by post annealing treatment in vacuum condition. *Sol. Energy Mater. Sol. Cells* **2018**, *187*, 170−175.

(21) Li, Z.; Liang, X.; Li, G.; Liu, H.; Zhang, H.; Guo, J.; Chen, J.; Shen, K.; San, X.; Yu, W.; et al. 9.2%-efficient core-shell structured antimony selenide nanorod array solar cells. *Nat. Commun.* **2019**, *10*, No. 125.

(22) Polman, A.; Knight, M.; Garnett, E. C.; Ehrler, B.; Sinke, W. C. Photovoltaic materials: Present efficiencies and future challenges. *Science* **2016**, *352*, No. aad4424.

(23) Tao, J.; Hu, X.; Xue, J.; Wang, Y.; Weng, G.; Chen, S.; Zhu, Z.; Chu, J. Investigation of electronic transport mechanisms in Sb2Se3 thin-film solar cells. *Sol. Energy Mater. Sol. Cells* **2019**, *197*, 1−6.

(24) Guo, L.; Grice, C.; Zhang, B.; Xing, S.; Li, L.; Qian, X.; Yan, F. Improved stability and efficiency of CdSe/Sb2Se3 thin-film solar cells. *Sol. Energy* **2019**, *188*, 586−592.

(25) Sorb, Y. A.; Rajaji, V.; Malavi, P. S.; Subbarao, U.; Halappa, P.; Peter, S. C.; Karmakar, S.; Narayana, C. Pressure-induced electronic topological transition in Sb2S3. *J. Phys.: Condens. Matter* **2016**, *28*, No. 015602.

(26) Wang, C.; Zhu, X.; Nilsson, L.; Wen, J.; Wang, G.; Shan, X.; Zhang, Q.; Zhang, S.; Jia, J.; Xue, Q. In situ Raman spectroscopy of topological insulator Bi2Te3 films with varying thickness. *Nano Res.* **2013**, *6*, 688−692.

(27) Medles, M.; Benramdane, N.; Bouzidi, A.; Sahraoui, K.; Miloua, R.; Desfeux, R.; Mathieu, C. Raman and Optical Studies of spray pyrolysed Sb2S3 thin films. *J. Optoelectron. Adv. Mater.* **2014**, *16*, 726−731.

(28) Parize, R.; Cossuet, T.; Chaix-Pluchery, O.; Roussel, H.; Appert, E.; Consonni, V. In situ analysis of the crystallization process of Sb2S3 thin films by Raman scattering and X-ray diffraction. *Mater. Des.* **2017**, *121*, 1−10.

(29) Shongalova, A.; Correia, M. R.; Vermang, B.; Cunha, J. M. V.; Salomé, P. M. P.; Fernandes, P. A. On the identification of Sb2Se3 using Raman scattering. *MRS Commun.* **2018**, *8*, 865−870.

(30) Vadapoo, R.; Krishnan, S.; Yilmaz, H.; Marin, C. Electronic structure of antimony selenide (Sb2Se3) from GW calculations. *Phys. Status Solidi B* **2011**, *248*, 700−705.

(31) Vidal-Fuentes, P.; Guc, M.; Alcobe, X.; Jawhari, T.; Placidi, M.; Pérez-Rodríguez, A.; Saucedo, E.; Roca, V. I. Multiwavelength excitation Raman scattering study of Sb2Se3 compound: Fundamental vibrational properties and secondary phases detection. *2D Mater.* **2019**, *6*, No. 045054.

(32) Rousseau, D. L.; Bauman, R. P.; Porto, S. P. S. Normal mode determination in crystals. *J. Raman Spectrosc.* **1981**, *10*, 253−290.

(33) Liu, Y.; Eddie Chua, K. T.; Sum, T. C.; Gan, C. K. First-principles study of the lattice dynamics of Sb2S3. *Phys. Chem. Chem. Phys.* **2014**, *16*, 345−350.

(34) Wiemer, C.; Ferrari, S.; Fanciulli, M.; Pavia, G.; Lutterotti, L. Combining grazing incidence X-ray diffraction and X-ray reflectivity for the evaluation of the structural evolution of HfO2 thin films with annealing. *Thin Solid Films* **2004**, *450*, 134−137.
(35) Momma, K.; Izumi, F. VESTA 3 for three-dimensional visualization of crystal, volumetric and morphology data. *J. Appl. Crystallogr.* **2011**, *44*, 1272−1276.
(36) Ivanova, Z. G.; Cernoskova, E.; Vassilev, V. S.; Boycheva, S. V. Thermomechanical and structural characterization of GeSe2-Sb2Se3-ZnSe glasses. *Mater. Lett.* **2003**, *57*, 1025−1028.
(37) Debernardi, A. Phonon linewidth in III-V semiconductors from density-functional perturbation theory. *Phys. Rev. B: Condens. Matter Mater. Phys.* **1998**, *57*, 12847−12858.
(38) Sereni, P.; Musso, M.; Knoll, P.; Blaha, P.; Schwarz, K.; Schmidt, G. Polarization-Dependent Raman Characterization of Stibnite (Sb2S3). *AIP Conf. Proc.* **2010**, *1267*, 1131−1132.
(39) Ibáñez, J.; Sans, J. A.; Popescu, C.; López-Vidrier, J.; Elvira-Betanzos, J. J.; Cuenca-Gotor, V. P.; Gomis, O.; Manjón, F. J.; Rodríguez-Hernández, P.; Muñoz, A. Structural, Vibrational, and Electronic Study of Sb2S3 at High Pressure. *J. Phys. Chem. C* **2016**, *120*, 10547−10558.
(40) Nagata, K.; Ishibashi, K.; Miyamoto, Y. Raman and infrared spectra of rhombohedral selenium. *Jpn. J. Appl. Phys.* **1981**, *20*, 463−469.
(41) Benjamin, S. L.; De Groot, C. H.; Hector, A. L.; Huang, R.; Koukharenko, E.; Levason, W.; Reid, G. Chemical vapour deposition of antimony chalcogenides with positional and orientational control: Precursor design and substrate selectivity. *J. Mater. Chem. C* **2015**, *3*, 423−430.
(42) Li, G.; Li, Z.; Chen, J.; Chen, X.; Qiao, S.; Wang, S.; Xu, Y.; Mai, Y. Self-powered, high-speed Sb2Se3/Si heterojunction photodetector with close spaced sublimation processed Sb2Se3 layer. *J. Alloys Compd.* **2018**, *737*, 67−73.
(43) Liu, X.; Chen, J.; Luo, M.; Leng, M.; Xia, Z.; Zhou, Y.; Qin, S.; Xue, D. J.; Lv, L.; Huang, H.; et al. Thermal evaporation and characterization of Sb2Se3 thin film for substrate Sb2Se3/CdS solar cells. *ACS Appl. Mater. Interfaces* **2014**, *6*, 10687−10695.
(44) Zhang, Y.; Li, G.; Zhang, B.; Zhang, L. Synthesis and characterization of hollow Sb2Se3 nanospheres. *Mater. Lett.* **2004**, *58*, 2279−2282.
(45) Zhou, Y.; Leng, M.; Xia, Z.; Zhong, J.; Song, H.; Liu, X.; Yang, B.; Zhang, J.; Chen, J.; Zhou, K.; et al. Solution-processed antimony selenide heterojunction solar cells. *Adv. Energy Mater.* **2014**, *4*, No. 1301846.
(46) Cody, C. A.; Dlcarlo, L.; Darlington, R. K. Vibrational and Thermal Study of Antimony Oxides. *Inorg. Chem.* **1979**, *18*, 1572−1576.
(47) An, D.; Chen, S.; Lu, Z.; Li, R.; Chen, W.; Fan, W.; Wang, W.; Wu, Y. Low Thermal Conductivity and Optimized Thermoelectric Properties of p-Type Te-Sb2Se3: Synergistic Effect of Doping and Defect Engineering. *ACS Appl. Mater. Interfaces* **2019**, *11*, 27788−27797.
(48) *Inorganic Crystal Structure Database*, File no. 194837; Fiz Karlsruhe, 2021.
(49) *Inorganic Crystal Structure Database*, File no. 240207; Fiz Karlsruhe, 2021.
(50) *Inorganic Crystal Structure Database*, File no. 4803; Fiz Karlsruhe, 2021.
(51) *Inorganic Crystal Structure Database*, File no. 85084; Fiz Karlsruhe, 2021.
(52) *Inorganic Crystal Structure Database*, File no. 157724; Fiz Karlsruhe, 2021.
(53) *Inorganic Crystal Structure Database*, File no. 41490; Fiz Karlsruhe, 2021.

https://doi.org/10.1021/acs.jpcc.1c05047
J. Phys. Chem. C 2021, 125, 19858−19865